Interplay of electronic, magnetic, and structural properties of GdB_6 from first principles

Shaowen Xu,[1] Fanhao Jia,[1] Yali Yang,[2] Lei Qiao,[1] Shunbo Hu,[1,3] David J. Singh,[4] and Wei Ren[1,3,*]

[1]*Physics Department, International Centre of Quantum and Molecular Structures, and State Key Laboratory of Advanced Special Steel, Shanghai University, Shanghai, 200444 China*

[2]*Key Laboratory of Computational Physical Sciences (Ministry of Education), State Key Laboratory of Surface Physics, and Department of Physics, Fudan University, Shanghai 200433, People's Republic of China*

[3]*Materials Genome Institute, and Shanghai Key Laboratory of High Temperature Superconductors, Shanghai University, Shanghai, 200444 China*

[4]*Department of Physics and Astronomy, University of Missouri, Columbia Missouri 65211–7010, USA*

(Received 16 May 2019; revised manuscript received 4 August 2019; published 4 September 2019)

Gadolinium hexaboride (GdB_6) is a well-known field emitter material that has been investigated for more than three decades. We perform a systematical density-functional theory study of GdB_6 by using the generalized-gradient approximation and considering the electron interaction parameter U. The basic structural and electronic properties are carefully revised, as well as a strong U-value dependence in determining the antiferromagnetic (AFM) magnetic structures of Gd $4f$ electronic states. We found a small U ($0 \sim 3$ eV) showing the most consistent experimental ground-state properties, which gives rise to a magnetic structure with a ground state of C-AFM and a second stable E-AFM. Moreover, we find the distortion modes of boron octahedron play an important role in the interaction between spin and lattice structures in this system. These results will deepen our understanding of the boron-based correlated rare earth compounds.

DOI: 10.1103/PhysRevB.100.104408

I. INTRODUCTION

The rare earth hexaborides (RB_6) crystallize in the cubic CaB_6-type structure [1], in which individual metal atoms and boron octahedra are arranged in the CsCl structure. They present intriguing physical properties, such as low work function (∼2.4–2.6 eV), high thermal conductivity, superconductivity, heavy fermion behavior and high melting points [2–6]. For example, the metallic LaB_6, a well-known thermionic and field electron emission cathode material, becomes superconducting below 0.45 K [6,7]; PrB_6 is believed to be antiferromagnetic (AFM) at low temperatures [8]; NdB_6 has shown favourable field-emission performances [9,10]; EuB_6 is a ferromagnetic (FM) semiconductor with two ferromagnetic transitions [11,12]; CeB_6 shows heavy fermion behavior and is famous as a dense Kondo material [5]; and mixed valence SmB_6 is a known topological Kondo insulator [13,14] where strong fermions can exhibit topological surface states.

Among the rare earth hexaborides, gadolinium hexaboride (GdB_6) exhibits the lowest work function (∼1.5 eV) [15]. However, the magnetic properties of GdB_6 are puzzling as it is not easy to determine the magnetic structure by neutron scattering due to the high neutron absorption of both Gd and B. GdB_6 was thought to have at least two first-order AFM transition with Néel temperature $T_N = 15$ K and $T^* = 8$ K [16], respectively, from the electrical resistivity and magnetic torque studies [17,18]. Galera *et al.* performed an x-ray scattering experiment and observed a reflection at $(0, 0, \frac{1}{2})$ at the temperature between T_N and T^*. Below T^*, they found a second type of reflection observed at $(\frac{1}{2}, \frac{1}{2}, 0)$ that coexisted with the former reflection [19]. However, they had no idea about whether the reflections of $(\frac{1}{2}, \frac{1}{2}, 0)$ were from a C-AFM or crystallographic distortions. Kasuya believed that the $(\frac{1}{2}, \frac{1}{2}, 0)$ reflection was from a charge dipolar ordering due to a so-called exchange-pair Jahn-Teller effect [20], which called for further examination. In 2004, Luca *et al.* performed a neutron diffraction of this system [16], they observed a propagation vector $(\frac{1}{4}, \frac{1}{4}, \frac{1}{2})$ with a basis magnetic moment direction vector $(0, 0, \frac{1}{2})$ at both 2 and 12 K, namely an E-AFM magnetic phase. However, no abnormalities around T^* were observed in their experiments. One year later, Amara *et al.* performed a mean-field model investigation combined with their x-ray scattering results indicating the coexistence of magnetic and displacement waves [21]. They supposed that the displacement waves imposed by the magnetic $(\frac{1}{4}, \frac{1}{4}, \frac{1}{2})$ structures are consistent with the $(0, 0, \frac{1}{2})$, $(\frac{1}{2}, \frac{1}{2}, 0)$, and $(\frac{1}{4}, \frac{1}{4}, \frac{1}{2})$ satellites observed in the x-ray scattering. These complex ordering patterns are characteristic of local moments associated with Gd interacting with metallic conduction electrons that can provide a nontrivial ordering due to, for example, Fermi surface properties. This demands a first-principles approach to the problem that includes both localized electrons in Gd f states and itinerant electrons on the boron backbone.

In the past few decades, density functional theory (DFT) has become an indispensable tool in material sciences and is widely used in determining the electronic and magnetic interactions of materials. However, the available previous DFT studies of GdB_6 mainly focused on its structural, electronic, and optical properties. Singh *et al.* calculated the

*renwei@shu.edu.cn

 ©2019 American Physical Society

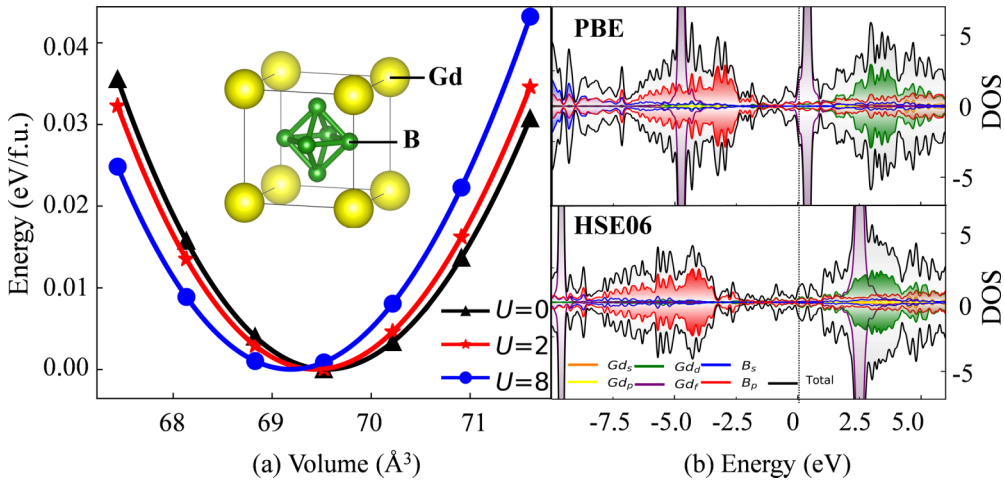

FIG. 1. (a) The energy values of PBE with $U = 0$, 2, 8 eV versus the volume per formula unit (f.u.). The inset shows the cubic structure of GdB_6. (b) The total and projected densities of states (DOS) of C-AFM GdB_6, the upper and lower panels are the PBE and HSE06 results, respectively.

reflectivity and optical conductivity of FM RB_6 using the LSDA + U method [15] but neglected the AFM or paramagnetic state. Furthermore, the selected U value (9 eV) of Gd directly obtained from previous studies on Gd_2O_3 requires some justification [22,23]. Li *et al.* indicated that GdB_6 is an almost perfect near-infrared absorption/reflectance material that could serve as a solar radiation shielding material for windows with high visible light transmittance [24]. They found that the magnetic $4f$ electrons of Gd are not relevant to the important optical properties of GdB_6, but the neglection of the AFM nature and the Hubbard U effect on $4f$ electrons needs to be further discussed. It is therefore crucial to perform a systematical DFT study to emphasize the AFM nature of GdB_6, to better understand how to utilize GdB_6, especially determining the magnetic ground state and revealing the interaction between the spin and lattice, and provide reasonable basic parameters for further research.

In this work, we fill these gaps in determining the magnetic structures of GdB_6 from first-principles calculations. The structural properties and electronic structure were carefully investigated, which are in good agreement with experimental value even at the GGA level. However, a strong U-value dependence of the magnetic structures and $4f$ electronic states is found and discussed in detail.

II. COMPUTATIONAL DETAILS

We performed the spin polarized calculations with the projector augmented wave approach [25,26], which were implemented in the Vienna *ab initio* simulation package (VASP) [27]. The $5p$, $6s$, $4f$, and $5d$ were taken as valence states for Gd, and $2s$ and $2p$ valence states were taken for B, respectively. The exchange correlation functional of generalized gradient approximation (GGA) was in the form proposed by Perdew, Burke, and Ernzerhof (PBE) [28], and an additional on-site interaction U [29] were realized in the form introduced by Dudarev *et al.* The convergence criterion of energy in relaxation was set to be 10^{-6} eV and atomic positions were fully relaxed until the maximum force on each atom was less than 10^{-3} eV/Å. The plane-wave cutoff energy is set to be 600 eV for all calculations. This represents a highly converged basis set. The precision of the total energy is set to be 10^{-8} eV. A $6 \times 6 \times 6$ Γ centered Monkhorst-Pack k mesh in the Brillouin zone was used here, where the convergence of k mesh were confirmed to be less 0.1 meV/atom. A $2 \times 2 \times 2$ superlattice (containing 56 atoms) was adopted to construct various magnetic configurations (the schematic diagrams displayed in Fig. S1) [30], which are six AFM orders (A, C, D, E, F, G-AFM) and a FM ordered state. The spin-orbit coupling (SOC) effect on the magnetic structures was examined, although it is expected to be weak due to the half filled f shell of Gd. The bulk modulus was obtained from fitting the Birch-Murnaghan equation of state. Furthermore, the screened hybrid functional proposed by Heyd, Scuseria, and Ernzerhof (HSE06) [31] was applied to investigate electronic properties, which has shown to be successful in a whole range of materials. The mixing of HF:GGA ratio was 0.25:0.75 and a screening parameter of 0.2 $Å^{-1}$ was adopted.

III. RESULTS AND DISCUSSION

A. Basic structural and electronic properties of cubic GdB_6

The simple cubic structure of GdB_6, space group $Pm\bar{3}m$ (No. 221), is displayed in Fig. 1(a). The boron octahedron is constructed by 6 B atoms and 12 B-B covalent bonds and the B_6 octahedron is located at the center of a cubic Gd lattice. We find that both the PBE calculated volume (69.53 $Å^3$) and bulk modulus (169 GPa) agree very well with the experimental values of 69.58 $Å^3$ and ~170 GPa [32]. Figure 1(b) shows the total and projected densities of states (PDOS) form PBE and HSE methods, where partially filled $4f$ orbitals are observed indicating the trivalent nature of Gd^{3+} consistent with previous reflectivity spectra measurement [33]. On the other hand, we find that the PDOS of B atoms has contributions to the total DOS in the whole displayed energy range, and a strong sp^3 hybridization behavior of the B octahedra is observed (see the

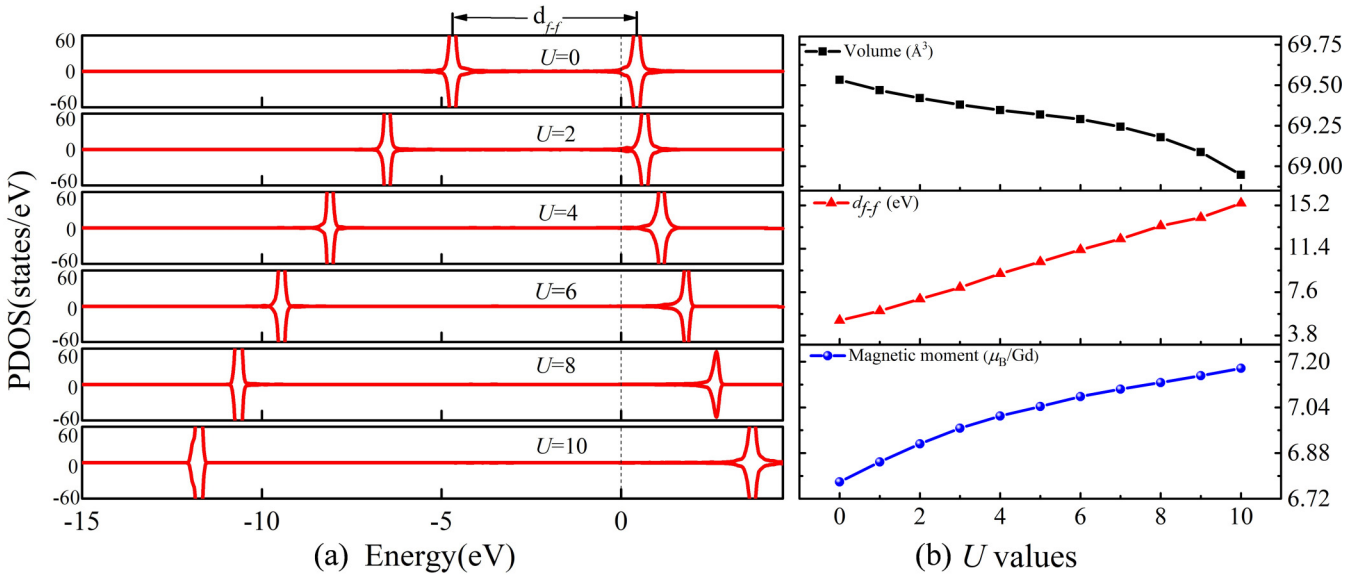

FIG. 2. (a) The f orbitals PDOS of GdB_6 under various U values. (b) The magnetic moment, volume and d_{f-f} versus U values are displayed, where d_{f-f} is defined as the separation between the peaks of two f orbitals. Here, we use the C-AFM system as a representative.

charge density map diagrams displayed in Fig. S2) [34], which shows that the B octahedra have strong relative stability.

Near the Fermi level, we find that both PBE and HSE show partially occupied Gd_d orbitals, which hybridize with the B states. These are the active electronic states for transport. In addition, two localized Gd_f peaks are observed in two specific energy ranges, namely the occupied one with PBE: $-4.5 \sim -5$ eV (HSE:$-9 \sim -9.5$ eV) and the unoccupied one with PBE: $0 \sim 0.6$ eV (HSE: $2.3 \sim 2.9$ eV), respectively. These are the exchange split majority and minority spin Gd f states. Note that already at the PBE level the exchange splitting is sufficient to fully polarize the Gd f shell. The HSE gives an extremely large and unreasonable energy splitting about 12 eV of two orbitals, which is more than two times of the PBE results. This overestimation is due to the simplistic treatment of the exchange functional rooted in the original Fock exchange energy, which is also found in Ce_2O_3 system [35] where the PBE0 (HSE06) overestimate up to 45% (15%) of the Ce $4f$ - $5d4f$ energy gap.

To deal with the well-known errors in the DFT, we also performed the GGA $+ U$ calculations for this system. The additional U increases the energy separation between the minority and majority f states. Figure 2(a) shows that the Hubbard U in particular pushes unoccupied f orbitals away from the Fermi level, while at the same time increasing the binding energy of the majority spin states as illustrated in Fig. 2(b). The U value not only changes the f states dramatically, but also alters the GdB_6 structure, electronic properties, and

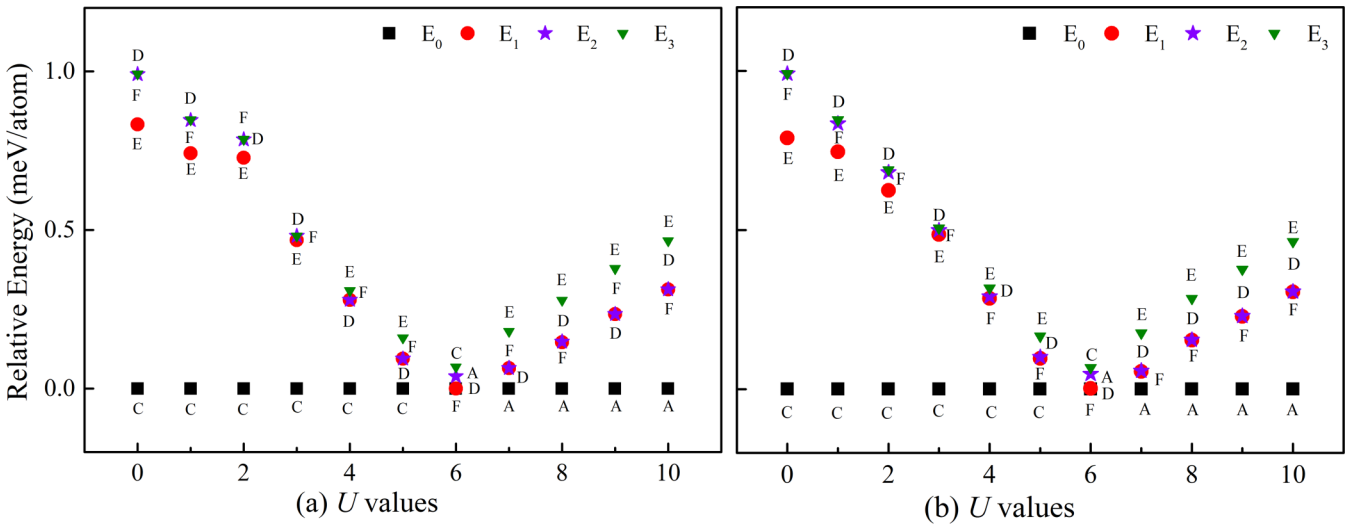

FIG. 3. The relative energy of various AFM configurations from (a) GGA $+ U$ and (b) GGA $+ U +$ SOC calculations, where the E_0, E_1, E_2, and E_3 represent the ground state energy, the first, second, and third higher energy state energies, respectively, which are represented by different colors and symbols. The corresponding magnetic structures are also indicated beside each symbol.

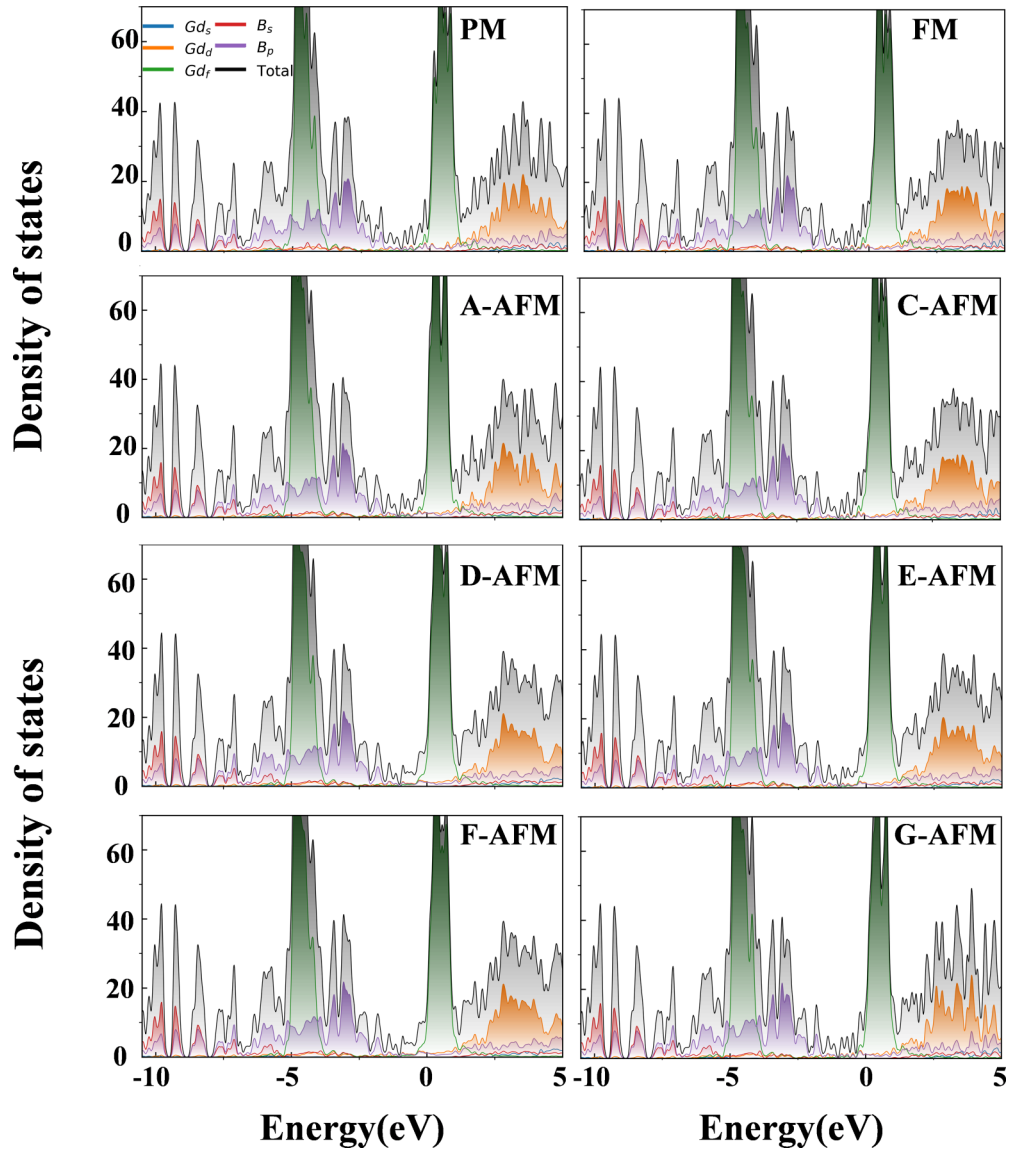

FIG. 4. The projected density of states of PBE calculations for paramagnetic (PM), FM, and six AFM phases of GdB_6.

magnetic properties. We find that the volume reduces monotonically when the U value increases, while the magnetic moment increases with the U value. The magnetic moment of Gd^{3+} obtained by us is within an integration sphere as in standard VASP calculations. We also note that the quoted magnetic moments are spin moments, since the half full shell of Gd does not allow significant orbital components. When the $U = 2$ eV, it agrees best with the experimental value $6.9\mu_B$ [16], which was derived with a Bragg R factor $= 2.7$ and a magnetic R factor $= 15$. Hence, the small U value range ($0\text{ eV} \leqslant U \leqslant 2\text{ eV}$) might be more favorable in the prediction of the structure, bulk modulus and its magnetic moment. A small $U_{\text{eff}} \approx 2.0$ eV value for GGA was also found to give the best overall description for the energetics, lattice constants, and magnetic ordering in the Ce_2O_3 system [35], instead of the calculated value of 4.50 eV from the linear-response approach [36]. As emphasized recently by us, that would lead to poor ground state properties in simple materials like Fe [37]. Another reason for using smaller U values is that the recent constrained random phase approximation calculations [38] of many rare earth nickelates [39] tend to favor smaller U values toward the f orbitals of these systems.

B. Low temperature magnetic structures

Figure 3(a) shows the GGA+U results of the relative energy of various AFM orderings, where we find C-AFM maintains as the ground magnetic structure until the U is larger than 5 eV. Then after an intermediate F-AFM at $U =$ 6 eV, the ground magnetic structure becomes A-AFM in the wide U value range. We also examine the SOC effect on the magnetic structures in Fig. 3(b). The SOC has no change in the ground magnetic structure, and only slightly shifts the relative energy of D-AFM and F-AFM within the calculational error. As mentioned, this weak SOC effect is consistent with the fully polarized f shell, which precludes orbital moments. On the other hand, the subground magnetic structure is more dependent on the chosen U values. The subground magnetic

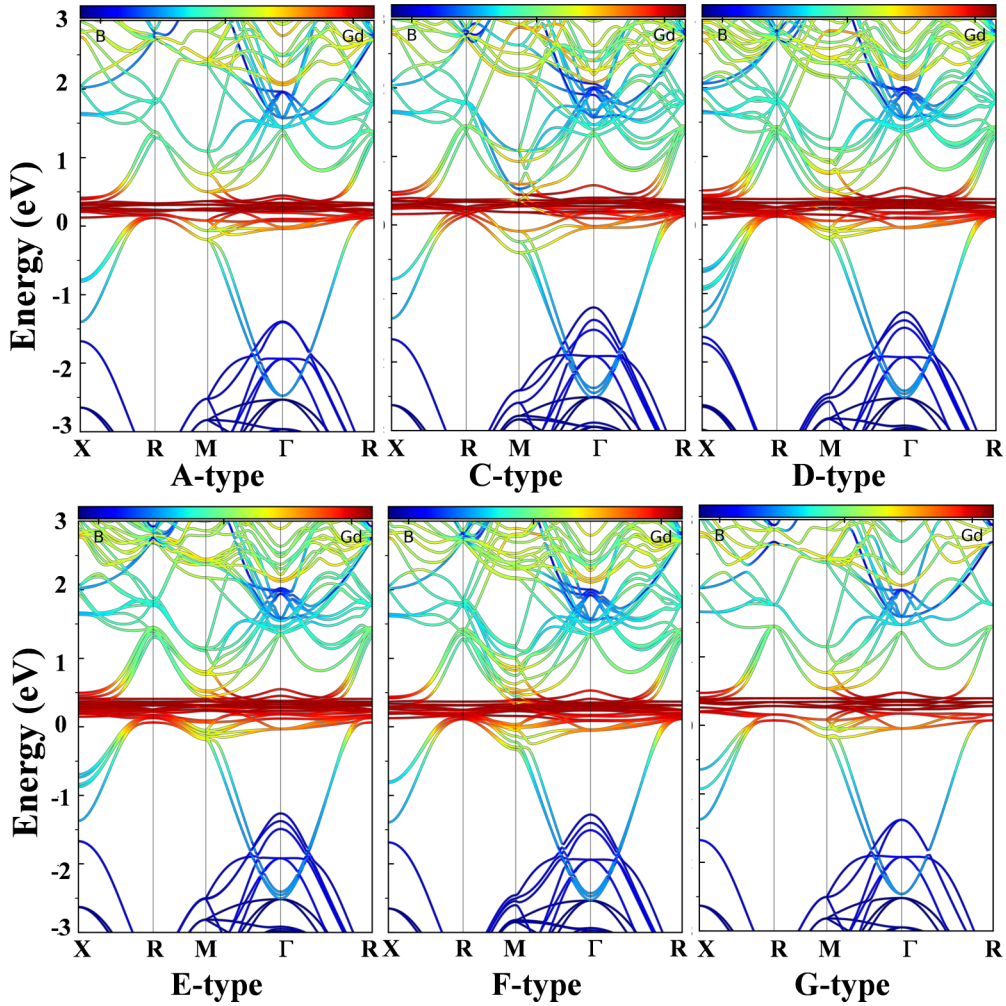

FIG. 5. The projected band structures of GGA calculations for six AFM phases of GdB_6.

structure favors the E-AFM in a small U value range ($U \leqslant 3$ eV), while it favors F-AFM or D-AFM in the large U value range.

As discussed above, a small U value ($U \leqslant 2$ eV) allows us to closely reproduce the experimental volume, bulk modulus, and magnetic moment. We also find the subground magnetic structure E-AFM is consistent with the experimental satellite observed in $(\frac{1}{4}, \frac{1}{4}, \frac{1}{2})$ at 12 K. Furthermore, the relative energy difference between E-AFM and C-AFM is from 1 meV/atom ($U = 0$ eV) to 0.6 meV/atom ($U = 2$ eV), corresponding to about 12–6 K in the temperature scale. Therefore, combining our DFT calculations with the small U value range and previous experiments, we think that there may indeed be a lower-energy magnetic state than E-AFM, namely the C-AFM. Such C-AFM ground structure is consistent with the $(\frac{1}{2}, \frac{1}{2}, 0)$ satellites observed in scattering experiments. The occurance of this state is connected with a relatively low value of U in our calculations. Such low values of U favor increased interaction between itinerant electrons and the Gd f local moments. On the other hand, higher values of U, which lead to stronger localization of the f states, would lead to the A-AFM state. Therefore, the combination of spectroscopic and magnetic measurements may provide insights into the magnetic behavior and its origins in this compound.

C. The influence of magnetic structure on the electronic structure and lattice distortion

The electronic DOS for various magnetic structures are shown in Fig. 4. These are very similar to each other below the Fermi level. However, the unoccupied states show quite different distributions, for instance, the paramagnetic (PM) and G-AFM configurations tend to have sharper peaks in the 3–3.5 eV energy range. These different unoccupied states are mainly derived from 5d states, hybridized with the boron backbone.

Band structures for various magnetic structures are given in Fig. 5. The dispersive bands below the Fermi level come from the mixing of Gd d and B states, showing small effective mass for all AFM configurations. The low effective mass emphasizes the itinerancy of this system, as does the experimentally observed conductivity. We also notice the dispersions of these bands are sensitive to the particular AFM order. This is consistent with the fact that charge transport anisotropy is observed in recent low temperature experiments

TABLE I. The lattice volume and bulk modulus of the GdB_6 calculated by using GGA, GGA + U ($U = 2$ eV) and ($U = 8$ eV).

	Volume (Å^3)							B(GPa)
Type	A	C	D	E	F	G	FM	
GGA	69.55	69.53	69.51	69.55	69.53	69.54	69.53	169
$U = 2$ eV	69.42	69.42	69.42	69.42	69.41	69.42	69.41	171
$U = 8$ eV	69.18	69.17	69.18	69.18	69.19	69.17	69.18	173
Exp				69.19 [41]				170 [32]

[40] even though the crystal symmetry without magnetism would preclude anisotropy.

In Table I, we list the calculated volume and bulk modulus for the different magnetic configurations of GdB_6. Similar to the electronic structures, the lattice parameters are sensitive to the magnetic order, though weakly so. This is shown in Fig. 6 . It is to be noted that the FM, PM, and G-AFM systems maintain the cubic crystal phase, while the other AFM orders investigated here lead to tetragonal crystal phase with space group $P4/mmm$ (No. 123).

In order to further study magnetoelastic distortions we combined our DFT results with the AMPLIMODES [42] analysis. We show the detailed distortion modes in Fig. 6 and list their normalized magnitudes in Table II. We find that the magnetic structures (A, C, D, E, and F-AFM) affect both the amplitudes and distortion modes, where the B octahedron is found to play an important role in the rich relationship between the spin and lattice. The A-AFM and C-AFM configurations only undergo two modes, namely the Γ_1^+ and Γ_3^+, while Γ_3^+ is the primary mode. These two modes are also observed in D, E, and F-AFM systems but with smaller magnitudes than other modes. As shown in Fig. 6, the Γ_1^+ mode displays the movements of all B atoms to the center of the B octahedron, while in the Γ_3^+ mode four B atoms in the ab plane move towards the center whereas two B atoms along the c axis move away from the center of the B octahedron. The D-AFM and F-AFM are similar to each other, as they undergo another primary mode M_1^+ together with the relatively small Γ_1^+ and Γ_3^+ modes. This M_1^+ mode is only contributed by the B atoms in the ab plane. The E-AFM configuration seems to be most complicated, where two extra X_1^+ and X_2^+ modes are found in addition to the Γ_1^+, Γ_3^+, and M_1^+ modes. The in-plane B atoms displacements have similar patterns for the X_1^+ and X_2^+ modes, but the two apical B atoms show relatively opposite movements for the two modes. In summary, our results of distorted structures strongly suggest that the GdB_6 crystal should present tetragonal symmetry as the ground state induced by magnetic ordering, although it is

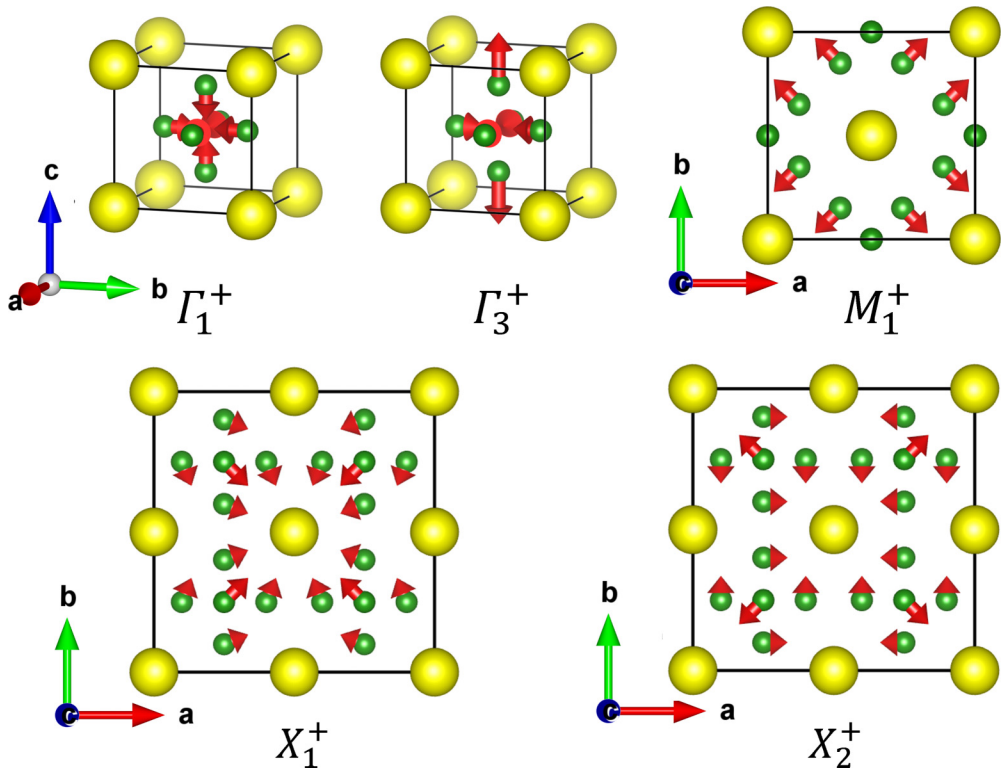

FIG. 6. Schematic illustration of the distortion modes of GdB_6. The red arrows represent the direction of the displacements. The magnitudes of the distortion modes are listed in Table II.

TABLE II. The input structures for AMPLIMODES analysis are evaluated within a symmetry tolerance of 10^{-4} Å. Mode amplitudes in distorted structures with different multiplication of their primitive unit cell are not directly comparable. The amplitudes are normalized with respect to the primitive unit cell of the high-symmetry structure by a normalization factor.

Type	Mode	k vector	Amplitude (10^{-4} Å)	Norm. factor	Global distortion (10^{-4} Å)
A	Γ_1^+	(0,0,0)	0	1	4
	Γ_3^+	(0,0,0)	4		
C	Γ_1^+	(0,0,0)	0	1	3
	Γ_3^+	(0,0,0)	3		
D	Γ_1^+	(0,0,0)	0	$\sqrt{2}$	8
	Γ_3^+	(0,0,0)	2		
	M_1^+	(1/2,1/2,1/2)	5		
E	Γ_1^+	(0,0,0)	0	2	19
	Γ_3^+	(0,0,0)	0		
	X_1^+	(0,1/2,0)	3		
	X_2^+	(0,1/2,0)	1		
	M_1^+	(1/2,1/2,1/2)	9		
F	Γ_1^+	(0,0,0)	0	$\sqrt{2}$	8
	Γ_3^+	(0,0,0)	2		
	M_1^+	(1/2,1/2,1/2)	5		

cubic at room temperature [18]. This is presumably the origin of the transport anisotropy.

IV. SUMMARY AND CONCLUSIONS

In summary, we have carried out first-principles calculations to investigate the geometric, electronic, and magnetic structure properties of GdB_6 with GGA and GGA + U methods. The $4f$ electronic states, structural, and magnetic properties are strongly dependent on the U value. We have found good agreement with the experimental results of magnetic moments, volume, and bulk modulus values in a U value range (0 eV $\leqslant U \leqslant$ 3 eV), in which the ground magnetic structure is C-AFM and the first higher-energy magnetic structure is E-AFM. However, in a wide U value range (5 eV $\leqslant U \leqslant$ 10 eV), the ground magnetic structure is found to be A-AFM. We find nontrivial spin-lattice coupling involving distortions of the B octahedra. Importantly, we also find a relationship between the magnetic order of the ground state and the strength of the on-site Coulomb interaction. It will be of interest to examine this in future experiments, for example,through combinations of scattering and photoemission spectroscopy.

ACKNOWLEDGMENTS

This work was supported by the National Natural Science Foundation of China (Grants No. 51672171, No. 51861145315, and No. 51911530124), the National Key Basic Research Program of China (Grant No. 2015CB921600), the fund of the State Key Laboratory of Solidification Processing in NWPU (SKLSP201703), the Austrian Research Promotion Agency (FFG, research Grant No. 870024, project acronym "MagnifiSens"). The Department for Integrated Sensor Systems also gratefully acknowledges partial financial support by the European Regional Development Fund (EFRE) and the province of Lower Austria. Work at the University of Missouri was supported by the U.S. Department of Energy, Award No. DE-SC0019114. The supercomputing services from AM-HPC, the Fok Ying Tung Education Foundation are also acknowledged.

[1] H. Hacker, Jr. and M. S. Lin, Solid State Commun. **6**, 379 (1968).
[2] B. Matthias, T. Geballe, K. Andres, E. Corenzwit, G. Hull, and J. Maita, Science **159**, 530 (1968).
[3] G. Schell, H. Winter, H. Rietschel, and F. Gompf, Phys. Rev. B **25**, 1589 (1982).
[4] N. Xu, C. E. Matt, E. Pomjakushina, J. H. Dil, G. Landolt, J.-Z. Ma, X. Shi, R. S. Dhaka, N. C. Plumb, M. Radović, V. N. Strocov, T. K. Kim, M. Hoesch, K. Conder, J. Mesot, H. Ding, and M. Shi, arXiv:1405.0165.
[5] T. Komatsubara, N. Sato, S. Kunii, I. Oguro, Y. Furukawa, Y. Ōnuki, and T. Kasuya, J. Magn. Magn. Mater. **31**, 368 (1983).
[6] H. Hagiwara, H. Hiraoka, R. Terasaki, M. Ishii, and R. Shimizu, Scanning Electron Microsc. **1982**, 473 (1982).
[7] K. Qi, Z. Lin, W. Chen, G. Cao, J. Cheng, and X. Sun, Appl. Phys. Lett. **93**, 093503 (2008).
[8] Y. Onuki, A. Umezawa, W. K Kwok, G. W Crabtree, M. Nishihara, T. Yamazaki, T. Omi, and T. Komatsubara, Phys. Rev. B **40**, 11195 (1989).
[9] J. Xu, G. Hou, T. Mori, H. Li, Y. Wang, Y. Chang, Y. Luo, B. Yu, Y. Ma, and T. Zhai, Adv. Funct. Mater. **23**, 5038 (2013).
[10] C. McCarthy and C. Tompson, J. Phys. Chem. Solids **41**, 1319 (1980).
[11] S. Patil, G. Adhikary, G. Balakrishnan, and K. Maiti, Solid State Commun. **151**, 326 (2011).

[12] M. C. Aronson, J. L. Sarrao, Z. Fisk, M. Whitton, and B. L Brandt, Phys. Rev. B **59**, 4720 (1999).
[13] M. Sundermann, H. Yavaş, K. Chen, D. J. Kim, Z. Fisk, D. Kasinathan, M. W. Haverkort, P. Thalmeier, A. Severing, and L. H. Tjeng, Phys. Rev. Lett. **120**, 016402 (2018).
[14] F. Lu, J. Z. Zhao, H. Weng, Z. Fang, and X. Dai, Phys. Rev. Lett. **110**, 096401 (2013).
[15] N. Singh, S. M. Saini, T. Nautiyal, and S. Auluck, J. Phys.: Condens. Matter **19**, 346226 (2007).
[16] S. Luca, M. Amara, R. Galéra, F. Givord, S. Granovsky, O. Isnard, and B. Beneu, Physica B **350**, E39 (2004).
[17] T. Tanaka, R. Nishitani, C. Oshima, E. Bannai, and S. Kawai, J. Appl. Phys. **51**, 3877 (1980).
[18] H. Nozaki, T. Tanaka, and Y. Ishizawa, J. Phys. C Solid State Phys. **13**, 2751 (1980).
[19] R. Galera, D. Osterman, J. Axe, S. Kunii, and T. Kasuya, J. Appl. Phys. **63**, 3580 (1988).
[20] T. Kasuya, J. Magn. Magn. Mater. **174**, L28 (1997).
[21] M. Amara, S. E. Luca, R.-M. Galéra, F. Givord, C. Detlefs, and S. Kunii, Phys. Rev. B **72**, 064447 (2005).
[22] H. Jamnezhad and M. Jafari, J. Comput. Electron. **16**, 272 (2017).
[23] P. Larson, W. R. L. Lambrecht, A. Chantis, and M. van Schilfgaarde, Phys. Rev. B **75**, 045114 (2007).
[24] L. Xiao, Y. Su, J. Ran, Y. Liu, W. Qiu, J. Wu, F. Lu, F. Shao, D. Tang, and P. Peng, J. Appl. Phys. **119**, 164903 (2016).
[25] C. J. Först, C. R. Ashman, K. Schwarz, and P. E. Blöchl, Nature (London) **427**, 53 (2004).
[26] G. Kresse and D. Joubert, Phys. Rev. B **59**, 1758 (1999).
[27] G. Kresse and J. Furthmüller, Phys. Rev. B **54**, 11169 (1996).
[28] J. P. Perdew, K. Burke, and M. Ernzerhof, Phys. Rev. Lett. **77**, 3865 (1996).
[29] V. I. Anisimov, J. Zaanen, and O. K. Andersen, Phys. Rev. B **44**, 943 (1991).
[30] See Supplemental Material at http://link.aps.org/supplemental/10.1103/PhysRevB.100.104408 for detailed information about the schematic of six antiferromagnetic structures (A, C, D, E, F, and G-AFM) in a $2 \times 2 \times 2$ superlattice.
[31] J. Heyd, G. E. Scuseria, and M. Ernzerhof, J. Chem. Phys. **118**, 8207 (2003).
[32] G. Grechnev, A. Logosha, A. Panfilov, and N. Y. Shitsevalova, J. Alloys Compd. **511**, 5 (2012).
[33] S.-i. Kimura, T. Nanba, S. Kunii, and T. Kasuya, Phys. Rev. B **50**, 1406 (1994).
[34] See Supplemental Material at http://link.aps.org/supplemental/10.1103/PhysRevB.100.104408 for detailed information about the charge density distribution of GdB_6.
[35] J. L. F. Da Silva, M. V. Ganduglia-Pirovano, J. Sauer, V. Bayer, and G. Kresse, Phys. Rev. B **75**, 045121 (2007).
[36] M. Cococcioni and S. de Gironcoli, Phys. Rev. B **71**, 035105 (2005).
[37] Y. Fu and D. J. Singh, Phys. Rev. B **100**, 045126 (2019).
[38] F. Aryasetiawan, M. Imada, A. Georges, G. Kotliar, S. Biermann, and A. I. Lichtenstein, Phys. Rev. B **70**, 195104 (2004).
[39] A. Hampel, P. Liu, C. Franchini, and C. Ederer, NPJ Quant. Mater. **4**, 5 (2019).
[40] M. Anisimov, V. Glushkov, A. Bogach, S. Demishev, N. Samarin, A. Samarin, N. Shitsevalova, A. Levchenko, V. Filipov, S. Gábani, K. Flachbart, and N. Sluchanko, Acta Phys. Pol. A **131**, 973 (2017).
[41] T. Y. Kosolapova, *Handbook of High Temperature Compounds: Properties, Production, Applications* (CRC Press, Boca Raton, FL, 1990).
[42] D. Orobengoa, C. Capillas, M. I. Aroyo, and J. M. Perez-Mato, J. Appl. Crystallogr. **42**, 820 (2009).